ISTITUTO NAZIONALE DI RICERCA METROLOGICA
Repository Istituzionale

Influence of Multilayer Architecture on the Structural, Optical, and Photoluminescence Properties of ZnO Thin Films

Original
Influence of Multilayer Architecture on the Structural, Optical, and Photoluminescence Properties of ZnO Thin Films / Malpure, Neha N.; Patil, Sumit R.; Sali, Jaydeep V.; Pugliese, Diego; Afre, Rakesh A.; Khadayate, Rajendra S.. - In: PHOTONICS. - ISSN 2304-6732. - 12:12(2025). [10.3390/photonics12121219]

Availability:
This version is available at: 11696/87439 since: 2025-12-10T14:31:08Z

Publisher:
MDPI

Published
DOI:10.3390/photonics12121219

Terms of use:

This article is made available under terms and conditions as specified in the corresponding bibliographic description in the repository

Publisher copyright

(Article begins on next page)

28 April 2026

Article

Influence of Multilayer Architecture on the Structural, Optical, and Photoluminescence Properties of ZnO Thin Films

Neha N. Malpure [1], Sumit R. Patil [2], Jaydeep V. Sali [3], Diego Pugliese [4,*], Rakesh A. Afre [5] and Rajendra S. Khadayate [1,*]

1 GDM Arts, KRN Commerce and MD Science College, Jalgaon Road, Near Bus Stand, Taluka, District Jalgaon, Jamner 424206, Maharashtra, India; nnmalpure@nmu.ac.in
2 Department of Electrical and Computer Engineering, Zeal College of Engineering and Research, Survey No. 39, Narhe-Dhayari Road, Narhe, Pune 411041, Maharashtra, India; sumit.patil@zealeducation.com
3 Department of Physics, Kavayitri Bahinabai Chaudhari North Maharashtra University, Umavi Nagar, Jalgaon 425001, Maharashtra, India; jvsali@nmu.ac.in
4 National Institute of Metrological Research (INRiM), Strada delle Cacce 91, 10135 Torino, Italy
5 School of Technology and Research, Dnyaan Prasad Global University, Sant Tukaram Nagar, District Pune, Pimpri 411018, Maharashtra, India; rakesh.afre@dypdpu.edu.in
* Correspondence: d.pugliese@inrim.it (D.P.); rskhadayate@gmail.com (R.S.K.); Tel.: +91-77982-58767 (R.S.K.)

Abstract

The present work systematically investigates the impact of multilayer architecture—specifically 5, 10, and 15 layers—on the structural, morphological, optical, and dielectric properties of zinc oxide (ZnO) thin films, aiming to tailor their characteristics for optoelectronic applications. The films were characterized using a comprehensive suite of techniques. X-ray diffraction (XRD) analysis of the 15-layer sample confirmed the formation of polycrystalline ZnO with a hexagonal wurtzite crystal structure, showing prominent (100), (002), and (101) diffraction peaks. Measurements indicated that the film thickness progressively increased from 43.81 nm for 5 layers to 80.68 nm for 15 layers. Concurrently, the surface roughness significantly decreased from 5.54 nm (5 layers) to 2.00 nm (15 layers) with increasing layer count, suggesting enhanced film quality and densification. Optical studies using ultraviolet–visible (UV-Vis) spectroscopy revealed an increase in absorbance and a corresponding decrease in transmittance in the UV-Vis spectrum as the film thickness increased. The calculated optical band gap showed a slight redshift, decreasing from 3.26 eV for the 5-layer film to 3.23 eV for the 15-layer film. Photoluminescence (PL) spectra exhibited characteristic near-band-edge UV emission, with the 5-layer film demonstrating the highest PL intensity. Furthermore, analysis of optical constants revealed that the refractive index, extinction coefficient, optical conductivity, and both the real and imaginary parts of the dielectric constant generally increased with an increasing number of layers, particularly in the visible region, while more nuanced and non-monotonic trends were observed in the UV range. These results underscore the significant influence of layer number on the physical properties of ZnO thin films, providing valuable insights for optimizing their performance in various optoelectronic devices.

Keywords: zinc oxide thin films; multilayer deposition; sol–gel process; thin film morphology; optical properties; photoluminescence; dielectric properties; optoelectronic materials; band gap engineering; refractive index

Received: 14 October 2025
Revised: 5 December 2025
Accepted: 9 December 2025
Published: 9 December 2025

Citation: Malpure, N.N.; Patil, S.R.; Sali, J.V.; Pugliese, D.; Afre, R.A.; Khadayate, R.S. Influence of Multilayer Architecture on the Structural, Optical, and Photoluminescence Properties of ZnO Thin Films. *Photonics* **2025**, *12*, 1219. https://doi.org/10.3390/photonics12121219

Copyright: © 2025 by the authors. Licensee MDPI, Basel, Switzerland. This article is an open access article distributed under the terms and conditions of the Creative Commons Attribution (CC BY) license (https://creativecommons.org/licenses/by/4.0/).

1. Introduction

Zinc oxide (ZnO), a versatile II–VI semiconductor, has attracted considerable scientific and technological interest due to its unique combination of physical and chemical properties. It crystallizes mainly in the wurtzite hexagonal structure, which lacks inversion symmetry and gives rise to strong piezoelectric and pyroelectric effects [1]. ZnO features a direct wide band gap of ~3.37 eV at room temperature and a large exciton binding energy of 60 meV, exceeding that of ZnS (20 meV) and GaN (25 meV) [2]. This high binding energy ensures efficient excitonic emission even at and above room temperature, making ZnO highly promising for optoelectronic applications. In addition, its abundance, low cost, and environmental compatibility enhance its potential for large-scale production [3]. Other advantageous properties include high electron mobility, good thermal conductivity, optical transparency in the visible range, and biocompatibility, enabling applications in transparent electronics, sensors, energy harvesting, and biomedical devices [4].

The fabrication of ZnO as thin films is particularly important for integration into modern electronic and optoelectronic devices. Thin films preserve most bulk properties while offering additional benefits such as compatibility with planar architectures, tunable characteristics through controlled deposition, and reduced material consumption [5]. A wide range of deposition techniques has been employed, including pulsed laser deposition (PLD) [6], chemical vapor deposition (CVD) [7], magnetron sputtering [8], atomic layer deposition (ALD) [9], spray pyrolysis [10], and sol–gel methods [11]. Among these, sol–gel deposition combined with layer-by-layer approaches such as spin or dip coating stands out for its low cost, compositional control, scalability, and operation under ambient conditions, making it suitable for both research and industrial applications [12].

The physical, structural, and optical characteristics of ZnO thin films are strongly influenced by thickness. As films grow, their microstructure evolves—affecting crystal orientation, grain size, surface morphology, and defect density. For ZnO, thicker films typically show improved crystallinity and stronger *c*-axis (002) orientation, the most stable growth direction of the wurtzite phase [13–15]. Such structural evolution directly impacts optical and electronic properties: for instance, the optical band gap can be tuned with thickness due to quantum confinement effects in ultrathin layers, strain relaxation, and changes in localized states near the band edges [16,17].

A thorough understanding of how thickness affects ZnO film properties is thus essential for device design. Parameters such as the refractive index (n) and extinction coefficient (k)—crucial for antireflection coatings and optical waveguides—are highly sensitive to film density and surface roughness [18]. Photoluminescence (PL) spectroscopy further provides insight into electronic structure and defect states, with the UV-to-visible emission ratio commonly used as an indicator of optical quality. This ratio varies with thickness due to changes in oxygen vacancies, surface states, and other point defects [19,20]. Similarly, the Urbach energy (E_u), which reflects the extent of structural disorder, serves as a quantitative measure of crystalline quality and is also thickness-dependent. While many studies have examined individual properties as a function of thickness, a systematic, correlative investigation linking structural, morphological, optical, and luminescent behavior during layer-by-layer growth is still needed [21].

The present work addresses this gap by systematically analyzing ZnO thin films with varying numbers of sol–gel-deposited layers (5, 10, and 15). Their crystalline structure, surface morphology, thickness, and roughness are examined, together with a detailed characterization of optical properties, including transmittance, absorbance, band gap energy, refractive index, extinction coefficient, dielectric constants, and optical conductivity. Defect-related dynamics are evaluated through Urbach energy and photoluminescence spectra. By correlating these measurements, a comprehensive view is obtained of how ZnO

thin film properties evolve during early and intermediate growth stages, providing insights relevant for the tailored fabrication of ZnO-based devices.

The novelty of this study lies in its integrative approach, directly linking structural order (XRD and Urbach energy) to optical constants and PL response. In particular, a distinctive trend of decreasing surface roughness with increasing thickness is observed, pointing to a surface-smoothing growth mechanism. This holistic perspective offers a clearer understanding of defect dynamics in ZnO thin films and their impact on performance-critical properties. In contrast to conventional thickness-series studies based on a single continuous deposition, here the thickness is adjusted through a controlled multilayer (repeated spin coating) process. This approach promotes gradual densification and surface smoothing between cycles, potentially leading to microstructural differences that go beyond a simple increase in total thickness.

2. Materials and Methods

2.1. Materials

Zinc oxide thin films were synthesized using the sol–gel method combined with spin coating, as illustrated in the flowchart reported in Figure 1. For the sol preparation, zinc acetate dihydrate [$Zn(CH_3COO)_2 \cdot 2H_2O$] (Sigma-Aldrich, St. Louis, MO, USA) was employed as the zinc oxide precursor, 2-methoxyethanol (Qualigens, Thermo Fisher Scientific India Pvt. Ltd., Mumbai, India) was used as the solvent, and diethanolamine (Rankem, Avantor Performance Materials India Ltd., Thane, India) served as the stabilizing agent.

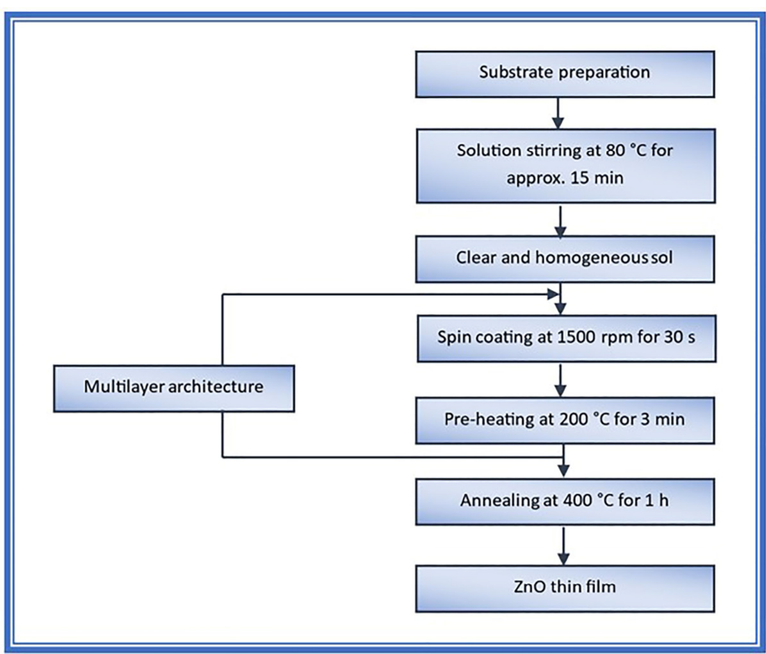

Figure 1. Schematic representation of the ZnO thin film synthesis process.

2.2. Synthesis of ZnO Thin Films

A measured amount of zinc acetate dihydrate was dissolved in 25 mL of 2-methoxyethanol and stirred at 80 °C until the solution turned milky. A few drops of diethanolamine were then added, resulting in a clear and transparent solution, which was stirred for an additional hour at 80 °C. The resulting sol was stored in a covered beaker at room temperature for 24 h. Prior to deposition, glass substrates were cleaned using an ultrasonic bath. The substrates were mounted on a spin coater, rotated at 1500 rpm, and pre-heated at 200 °C. The prepared sol was applied dropwise onto the substrate surface to form a film layer. This deposition procedure was repeated 5, 10, and 15 times to obtain ZnO

multilayers on glass substrates. The films adhered well to the substrate surface. Finally, three films were prepared and annealed at 400 °C for 1 h. These samples were subsequently used for further investigations. In this study, the term "multilayer architecture" refers to the repeated spin coating and pre-heating sequence characteristic of layer-by-layer sol–gel deposition, in which each wet layer is dried before the next is applied, and all layers are subsequently annealed to form a dense, continuous film rather than sharply separated sub-layers. For each nominal layer number (5, 10, and 15), multiple independently prepared films were fabricated and characterized. The structural and optical values reported correspond to representative averages obtained from these repeated depositions.

2.3. Characterization

The structural, optical, morphological, and photoluminescence properties of the synthesized ZnO thin films were comprehensively characterized. X-ray diffraction (XRD, Rigaku, Tokyo, Japan; CuKα, λ = 1.54059 Å) was carried out in the 2θ range of 20–80° to investigate the structural features. Optical absorbance and transmittance were recorded using a Shimadzu UV-1601 spectrophotometer (Shimadzu Corporation, Kyoto, Japan) in the wavelength range of 300–900 nm, while the film thickness was determined with a stylus surface profilometer (Dektak 150, Bruker Corporation, Billerica, MA, USA). More in detail, film thickness was obtained by measuring the step height across a small scratch made through the ZnO layer down to the glass substrate. The reported thickness values represent averages of several scans for each sample. The same profilometer, operated in surface-scanning mode, was used to estimate the root-mean-square (RMS) roughness, with the reported values calculated by averaging measurements from multiple regions to ensure reproducibility. Surface morphology was analyzed with a field-emission scanning electron microscope (FESEM, FEI Nova NanoSEM 450, FEI Company, Hillsboro, OR, USA) operating at 10 kV, and the luminescence behavior was studied using a FluoroMax-4 spectrofluorometer (Horiba Scientific, Kyoto, Japan).

3. Results and Discussion

3.1. Structural Characterization of ZnO Thin Films by X-Ray Diffraction

Figure 2 shows the XRD pattern of the 15-layer ZnO thin film, recorded at room temperature to examine its crystalline structure and phase purity. The diffraction pattern displays multiple well-defined peaks, confirming the polycrystalline nature of the synthesized film. The diffraction peaks observed at $2\theta \approx 31.8°$, 34.4°, 36.2°, 47.5°, 56.6°, 62.8°, and 67.9° correspond to the (100), (002), (101), (102), (110), (103), and (112) crystallographic planes, respectively. These peaks are in good agreement with standard data for the hexagonal wurtzite structure of ZnO [21]. The absence of additional peaks attributable to secondary phases or impurities indicates the successful formation of phase-pure ZnO within the detection limits of the technique. The corresponding wurtzite lattice parameters ($a \approx 3.25$ Å, $c \approx 5.20$ Å) describe the periodic atomic arrangement and remain essentially unchanged for all films; as such, they are not directly comparable to the total film thickness, which reflects the cumulative stacking of many such unit cells during layer-by-layer deposition. Additional XRD scans collected for the 5- and 10-layer films likewise confirmed phase-pure wurtzite ZnO with similar peak positions and relative intensities, although detailed analysis was limited to the 15-layer sample due to restricted instrument availability.

The relative intensities of the peaks provide information on preferred crystallographic orientation. In the recorded pattern, the (101) reflection exhibits the highest intensity, followed by the (002) and (100) peaks, with other reflections such as (102), (110), (103), and (112) appearing at lower intensities. According to standard Joint Committee on Powder Diffraction Standards (JCPDS) data, the (101) peak is typically the most intense

in randomly oriented polycrystalline ZnO, followed by (100) and (002). The dominance of the (101) reflection in the present film therefore suggests largely random orientation rather than a strong preferential alignment along the *c*-axis (002) plane, which is often desirable for specific optoelectronic applications [22]. Although the (002) peak is clearly visible, its relative intensity does not indicate a highly *c*-axis-textured film. The coexistence of multiple orientations may influence electrical conductivity, carrier transport, and surface morphology [23].

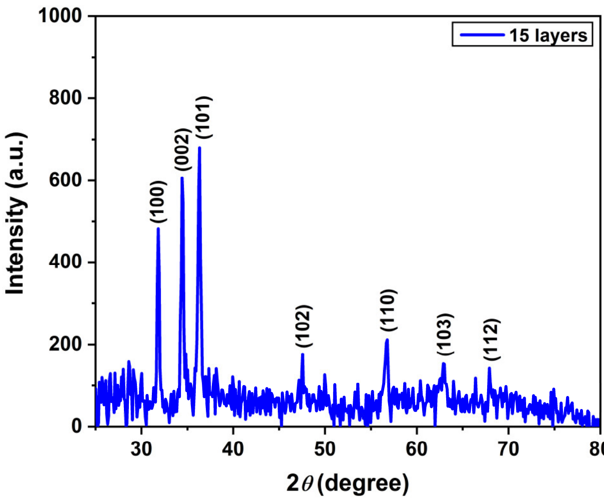

Figure 2. XRD pattern of the 15-layer ZnO thin film.

The sharp and well-defined nature of the diffraction peaks reflects good crystallinity. The average crystallite size can be estimated from the full width at half maximum (FWHM) of the reflections using the Debye–Scherrer equation:

$$D = \frac{K\lambda}{\beta \cos\theta}, \tag{1}$$

where D is the average crystallite size, K is the Scherrer constant (typically ~0.9), λ is the X-ray wavelength, β is the FWHM in radians, and θ is the Bragg diffraction angle [24]. Narrower peaks (smaller FWHM) correspond to larger crystallites and lower microstrain, generally indicative of improved crystalline quality. For the 15-layer film, the crystallite size estimated from the (101) reflection is in the range of 28–35 nm. The grains observed in the FESEM micrographs are slightly larger (≈40–50 nm), as expected since each surface grain typically consists of several coalesced crystallites. The multilayer architecture obtained through successive sol–gel spin coating cycles influences nucleation and growth kinetics, thereby affecting crystallite size and orientation [25]. Films with larger crystallites and fewer grain boundaries typically exhibit enhanced carrier mobility, beneficial for optoelectronic devices.

The structural features revealed by XRD—polycrystalline nature, phase purity, and good crystallinity—are crucial for assessing the potential performance of ZnO thin films in device applications. While a strong *c*-axis orientation is often favored for piezoelectric or light-emitting devices due to the anisotropic properties of ZnO, polycrystalline films with adequate crystallinity remain suitable for other applications such as transparent conductive oxides or ultraviolet (UV) photodetectors, provided grain boundary effects are controlled [26]. Further quantitative insight into preferred orientation could be obtained through the calculation of texture coefficients for the main reflections. Since such quantitative texture analysis was not performed in the present work, the discussion of preferred orientation is therefore kept qualitative.

3.2. Optical Properties

3.2.1. Absorbance Characteristics

The absorbance spectra of ZnO thin films with 5, 10, and 15 layers, shown in Figure 3a, exhibit typical semiconductor behavior. All films display low absorbance in the visible region (wavelengths > 400 nm) and a sharp increase in the UV region, particularly below ~390 nm. This pronounced absorption edge corresponds to the fundamental electronic transition in ZnO, where photons with energies exceeding the band gap excite electrons from the valence band to the conduction band [27].

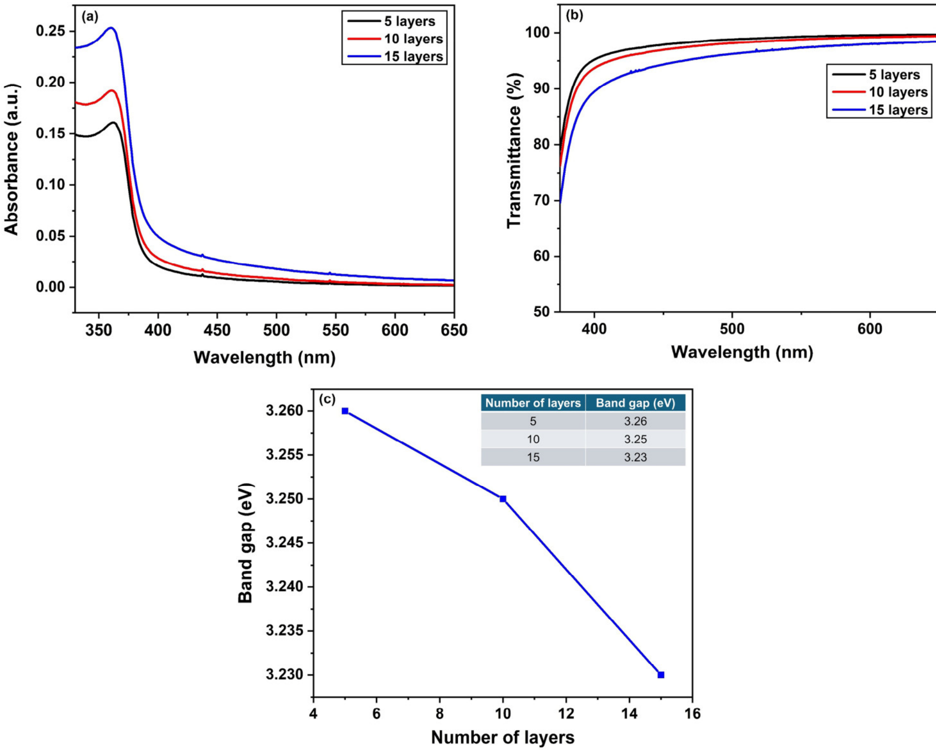

Figure 3. Optical characterization of multilayer ZnO films with 5, 10, and 15 layers: (**a**) absorbance spectra, (**b**) transmittance spectra, and (**c**) variation in the optical band gap with the number of layers.

A clear trend is observed with increasing film thickness: the overall absorbance intensity, especially near the UV absorption edge, rises as the number of layers increases from 5 to 10 and then to 15. This behavior is consistent with the Beer–Lambert law, which states that absorbance is directly proportional to the optical path length and the concentration of absorbing species [28]. Thicker films provide a longer optical path, enhancing photon absorption. Additionally, the absorption edge exhibits a slight redshift (toward longer wavelengths) with increasing thickness, suggesting a small decrease in the optical band gap, as quantified in Figure 3c. It should be emphasized that the stronger absorbance observed for thicker films primarily reflects the longer optical path length and multiple internal reflections, in addition to any thickness-induced microstructural changes.

Figure 3 summarizes the optical properties of ZnO thin films as a function of the number of deposited layers, which directly correlates with film thickness. Specifically, Figure 3a presents the absorbance spectra, Figure 3b shows the transmittance spectra, and Figure 3c illustrates the variation in the optical band gap for films with 5, 10, and 15 layers. These optical characteristics are critical for assessing the suitability of ZnO films for optoelectronic applications, including transparent conductive oxides, UV photodetectors, and solar cells.

3.2.2. Transmittance Properties

Figure 3b presents the percentage transmittance (%T) spectra of ZnO films with 5, 10, and 15 layers. In agreement with the absorbance data, all films exhibit high transparency in the visible range (400–800 nm), an essential characteristic for applications requiring transparent electrodes or window layers. The average transmittance in the visible region remains above 80–90% for thinner films, decreasing slightly with increasing film thickness. Specifically, the 5-layer film shows the highest transmittance, followed by the 10-layer film, while the 15-layer film displays the lowest transmittance across the visible spectrum. This decrease is attributed not only to possible improvements in film packing density but also to geometrical effects associated with a longer optical path.

This reduction in transmittance with increasing thickness is consistent with increased optical absorption and potential light scattering in thicker films, which may arise from larger grain sizes or higher surface roughness [29]. The pronounced drop in transmittance in the UV region corresponds to the fundamental absorption edge of ZnO, reflecting the behavior observed in the absorbance spectra. The combination of high visible transparency and strong UV absorption indicates that these ZnO films are suitable candidates for UV-shielding transparent coatings.

3.2.3. Optical Band Gap Variation

Figure 3c presents the calculated optical band gap (E_g) values as a function of the number of layers (5, 10, and 15). The results show a clear trend: the optical band gap decreases with increasing film thickness. Specifically, the band gap values are 3.26 eV for the 5-layer film, 3.25 eV for the 10-layer film, and 3.23 eV for the 15-layer film.

This slight reduction in band gap with increasing thickness can be attributed to several factors. For very thin films, quantum confinement effects can lead to a larger band gap; as thickness increases, these effects diminish, and the band gap approaches the bulk value or the characteristic value of thicker, more relaxed films [30]. Additionally, improvements in crystallinity and an increase in grain size with increasing thickness reduce defect-related localized states and band tailing, resulting in a slightly narrower and more well-defined band gap [5]. Variations in internal stress or strain as the film grows can further influence the electronic structure, with strain relaxation in thicker films contributing to the observed decrease in band gap [31]. Given the small magnitude of the shift ($\approx$0.03 eV), part of the apparent redshift may additionally arise from thickness-dependent interference and scattering. The band gap evolution should therefore be interpreted as the combined effect of intrinsic factors (crystallinity and strain) and extrinsic optical-path contributions.

The obtained band gap values are consistent with previously reported ranges for ZnO thin films (3.1–3.4 eV), which depend on deposition conditions, stoichiometry, and microstructure. These optical analyses indicate that increasing film thickness enhances UV absorption, slightly reduces visible transmittance, and decreases the optical band gap. The results highlight the crucial role of film thickness in tuning the optoelectronic properties of ZnO thin films for specific device applications.

3.2.4. Additional Optical Parameters

Figure 4 presents a detailed analysis of additional optical parameters of ZnO thin films deposited with 5, 10, and 15 layers, corresponding to different thicknesses. The examined parameters include refractive index (n), reflectance (%R), extinction coefficient (k), optical conductivity (σ_{opt}), and the real (ϵ_r) and imaginary (ϵ_i) components of the dielectric constant. These quantities are essential for describing light–matter interactions in the films and for assessing their suitability in optoelectronic applications. The analysis highlights their spectral dependence in the 350–700 nm wavelength range. Since the optical response of

ZnO thin films is critical for their integration into devices such as transparent conductive electrodes, solar cells, UV photodetectors, and light-emitting diodes, understanding the role of thickness is crucial. This section discusses how the variation in layer number (5, 10, and 15) affects the fundamental optical constants.

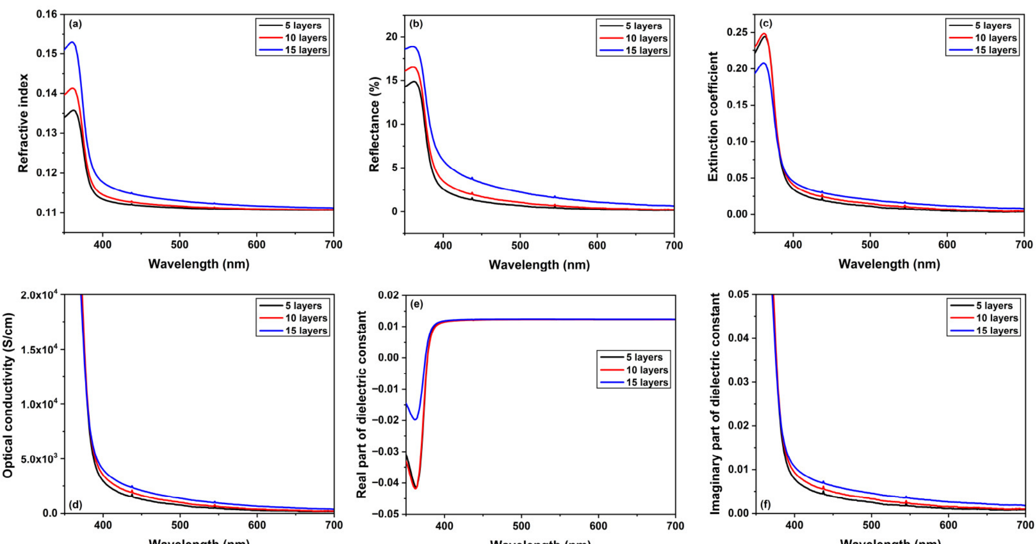

Figure 4. Spectral dependence of the optical parameters of ZnO thin films with 5, 10, and 15 layers: (**a**) refractive index (n), (**b**) percentage reflectance (%R), (**c**) extinction coefficient (k), (**d**) optical conductivity (σ_{opt}), (**e**) real part of the dielectric constant (ϵ_r), and (**f**) imaginary part of the dielectric constant (ϵ_i), all as functions of wavelength.

Figure 4a illustrates the spectral dependence of the refractive index (n) for ZnO films with 5, 10, and 15 layers. In the visible region (λ > 400 nm), n decreases gradually with increasing wavelength, showing normal dispersion. Approaching the UV region, near the fundamental absorption edge of ZnO (~380 nm), n rises sharply and exhibits a peak, indicating anomalous dispersion caused by resonant absorption processes [32]. Across the measured range, n increases systematically with film thickness: the 15-layer film consistently shows the highest values, followed by the 10- and 5-layer samples. At 550 nm, for instance, n slightly increases from 0.11097 (5 layers) to 0.11123 (10 layers) and 0.11224 (15 layers). This trend is generally attributed to higher packing density, improved crystallinity, and reduced porosity in thicker films, which typically feature larger grains and a more compact microstructure [33,34]. It should be noted, however, that the absolute values reported here (0.11–0.16) are unusually low compared to bulk ZnO ($n \approx 2.0$ in the visible region [25,26,28]). Such a discrepancy suggests a highly porous or nanostructured morphology with a low fill factor, or that the reported values correspond to effective-medium parameters within a specific optical model. Despite this, the progressive increase in n with increasing thickness remains a consistent indicator of structural evolution. Accordingly, the optical constants extracted in this work should be regarded as effective-medium values for a nanostructured, partially porous film within the assumed model, rather than intrinsic bulk ZnO parameters.

Figure 4b presents the percentage reflectance (%R) spectra. Reflectance is low in the visible range and rises steeply in the UV region, peaking near the absorption edge, in agreement with the spectral behavior of n and k. A clear thickness dependence is observed, with %R increasing with the number of layers. At 550 nm, reflectance is 0.427% for the 5-layer film, 0.670% for the 10-layer film, and 1.562% for the 15-layer film. This increase is consistent with Fresnel's equations, which predict higher reflectance for larger refractive indices, and may also be reinforced by interference effects that become more pronounced in

thicker films [35]. The low reflectance in the visible region is advantageous for applications requiring high transparency.

Figure 4c shows the extinction coefficient (k), which quantifies the attenuation of light through absorption or scattering within the film. As expected for ZnO, k is very low in the visible region, confirming high transparency, and increases sharply in the UV region below ~400 nm, corresponding to the onset of band-to-band absorption. Across the spectral range, k varies with the number of layers, particularly near the absorption edge. At 370 nm, for example, k decreases from ~0.218 (5 layers) to ~0.181 (15 layers). The observed reduction in k with increasing thickness suggests that thicker films have fewer defects and reduced scattering, consistent with improved crystallinity and grain growth [36]. The small but non-zero values observed in the visible region indicate residual absorption or scattering, likely associated with defects or grain boundaries.

Figure 4d presents the optical conductivity (σ_{opt}) as a function of wavelength. Optical conductivity reflects the material's ability to respond to an incident electromagnetic field through charge-carrier excitation. It is related to the absorption coefficient (α) and refractive index (n) by $\sigma_{opt} = \alpha nc/(4\pi)$, with $\alpha = 4\pi k/\lambda$ and c the speed of light. Accordingly, the spectral dependence of σ_{opt} closely follows that of k and the absorption coefficient. σ_{opt} remains low in the visible region and rises sharply in the UV region, particularly near the absorption edge. At 360 nm, the values are 2.7×10^4 S/cm (5 layers), 2.9×10^4 S/cm (10 layers), and 2.6×10^4 S/cm (15 layers). This trend indicates a modest thickness dependence, with a slight enhancement from 5 to 10 layers followed by a small reduction at 15 layers, which can be attributed to thickness-dependent microstructural evolution influencing carrier generation and scattering [37].

Figure 4e shows the real part of the dielectric constant (ϵ_r), which reflects the material's ability to store electrical energy from an incident electric field and is related to n and k by $\epsilon_r = n^2 - k^2$. The spectra exhibit dispersion near the UV absorption edge, with a sharp dip into negative values around 360 nm, followed by small positive values in the visible region. In the visible range, for example, at 550 nm, ϵ_r is positive and slightly increases with film thickness, from 0.01226 for the 5-layer film to 0.01236 for the 15-layer film. This trend follows that of n, as k is very small in this region, making $\epsilon_r \approx n^2$. The negative ϵ_r values in the UV region may arise from strong excitonic resonances or from significant free-carrier contributions leading to plasmonic behavior [38]. As a semiconductor, ZnO is expected to exhibit strong excitonic absorption near the band edge. The absolute values of ϵ_r, similar to n, are unusually low compared to bulk ZnO ($\epsilon_r \approx 3.7$–4.0 in the visible), reflecting the low refractive indices.

Figure 4f presents the imaginary part of the dielectric constant (ϵ_i), related to n and k by $\epsilon_i = 2nk$, which represents dielectric loss or energy absorption from the electric field. The spectral dependence of ϵ_i closely follows that of k and σ_{opt}, showing a steep increase in the UV region near the fundamental absorption edge, and very low values in the visible region. At 360 nm, ϵ_i is 0.0655 for the 5-layer film, 0.0699 for the 10-layer film, and 0.0634 for the 15-layer film. This trend indicates a modest thickness dependence, with a slight enhancement from 5 to 10 layers followed by a small reduction at 15 layers, reflecting thickness-dependent variations in optical absorption and energy dissipation.

The comprehensive analysis of the optical parameters shows trends with increasing film thickness that are consistent in the visible region and more nuanced in the UV region. In the visible, n, %R, and ϵ_r show slight increases with thickness, while k, σ_{opt}, and ϵ_i remain low. In the UV region, the behavior is not strictly monotonic: for example, at 360 nm, σ_{opt} and ϵ_i exhibit a slight enhancement from 5 to 10 layers and then a slight decrease at 15 layers, and k at 370 nm decreases with thickness. These observations reflect microstructural evolution: thicker films typically exhibit improved crystallinity, larger grain sizes, and

reduced porosity, resulting in a more "bulk-like" optical response, although the absolute values suggest a highly porous or nanostructured morphology [3,9,22]. The slight decrease in the optical band gap with thickness, observed previously (from 3.26 eV for 5 layers to 3.23 eV for 15 layers, see Figure 3), is consistent with structural improvements such as grain growth and strain relaxation, which influence the electronic band structure [10].

The observed optical characteristics—high visible transparency (low k and ϵ_i) and tunable UV absorption—are critical for ZnO-based optoelectronic devices. The systematic variation in these optical constants with thickness allows tailoring of film properties for specific applications. For transparent conductive oxide applications, high visible transmittance (low %R and k) and moderate optical conductivity are preferred, while for UV photodetectors, strong UV absorption (high k and σ_{opt}) is essential.

3.2.5. Urbach Energy Analysis of ZnO Thin Films with Varying Thickness

Figure 5 presents the determination of the Urbach energy (E_u) for ZnO thin films with 5, 10, and 15 layers. This parameter characterizes the width of the localized state tail extending from the band edges into the forbidden gap, originating from structural disorder, thermal vibrations, defects, and impurities in semiconductor materials [39].

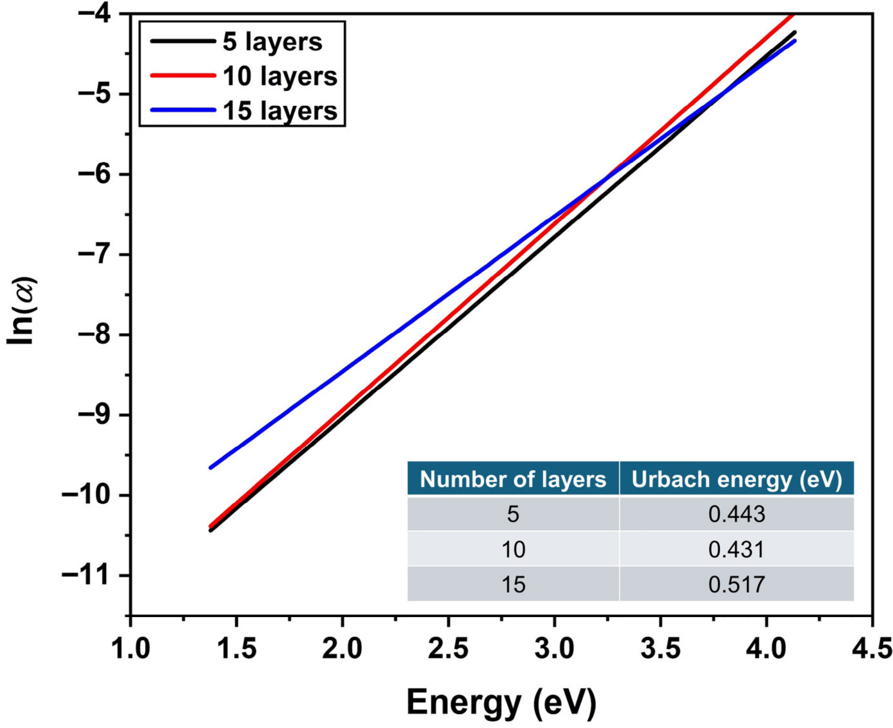

Figure 5. Plots of $\ln(\alpha)$ vs. photon energy ($h\nu$) for ZnO thin films with 5, 10, and 15 layers, with the inset table reporting the calculated Urbach energy values. This analysis provides insight into the degree of structural disorder and the distribution of localized states within the band gap.

A higher Urbach energy generally indicates greater structural disorder or a higher density of defects, which strongly affects the optical and electrical properties of the material. The analysis is carried out by plotting the natural logarithm of the absorption coefficient ($\ln(\alpha)$) against the photon energy ($h\nu$) in the sub-band gap region. According to the Urbach rule, the absorption coefficient follows an exponential dependence on photon energy:

$$\alpha\ (h\nu) = \alpha_0 \exp\left(\frac{h\nu}{E_u}\right), \tag{2}$$

where α_0 is a pre-exponential constant and E_u is the Urbach energy. Taking the natural logarithm yields:

$$\ln(\alpha) = \ln(\alpha_0) + \frac{h\nu}{E_u}. \tag{3}$$

Thus, E_u is obtained from the reciprocal slope of the linear portion of the $\ln(\alpha)$ vs. $h\nu$ plot.

The plots in Figure 5 show a linear relationship between $\ln(\alpha)$ and $h\nu$ below the fundamental absorption edge of ZnO (~3.2–3.3 eV) for all thicknesses (5, 10, and 15 layers), confirming the presence of an Urbach tail. The inset table reports the calculated values: 0.443 eV for 5 layers, 0.431 eV for 10 layers, and 0.517 eV for 15 layers. The trend is non-monotonic: as thickness increases from 5 to 10 layers, E_u decreases slightly (from 0.443 to 0.431 eV), suggesting improved structural order or reduced defect density [40]. Such improvement may result from enhanced atomic arrangement, grain growth, or strain relaxation, possibly aided by annealing effects during successive layer deposition [3]. A more ordered structure sharpens the band edges, reducing the Urbach tail.

For the 15-layer film, however, E_u rises markedly to 0.517 eV, indicating increased disorder, higher defect concentration, or a larger density of localized states. Contributing factors may include internal stress accumulation during extended deposition, leading to lattice distortions and defect formation, as well as a higher volume fraction of grain boundaries in polycrystalline films [41]. Additional impurities or growth-mode changes during prolonged deposition could further enhance disorder.

The magnitude of the measured Urbach energies is also significant. Values ranging from 0.431 to 0.517 eV are high compared to crystalline ZnO thin films, which typically exhibit E_u between 50 and 200 meV [12,26]. This suggests that all the films under study possess substantial disorder or defect density, possibly linked to high porosity or a nanostructured morphology. Such features are consistent with the unusually low refractive index values previously reported (Figure 4a), which point to a porous or less dense microstructure.

Since E_u quantifies disorder, its implications for optoelectronic performance are critical. A broad distribution of localized states near the band edges can trap charge carriers, lowering their mobility and lifetime, and promoting non-radiative recombination [42]. As a result, films with high E_u may suffer from reduced efficiency in solar cells (due to recombination losses), slower response or lower sensitivity in photodetectors, and decreased quantum efficiency in light-emitting diodes. The non-monotonic dependence of E_u on thickness suggests the existence of an optimal range (around 10 layers in this case) where structural disorder is minimized. Nonetheless, the relatively high E_u values overall indicate that further optimization of deposition conditions is required to enhance crystallinity and reduce defect density for high-performance optoelectronic applications. At the same time, part of the variation in Urbach energy may also arise from thickness-dependent optical scattering and interference, meaning that the separation between intrinsic structural disorder and optical-path effects is not yet complete. A more definitive distinction between these contributions would require complementary measurements—such as temperature-dependent and time-resolved photoluminescence—which are beyond the scope of the present work and are planned for future studies.

3.3. Surface Morphology and Qualitative Analysis

The surface morphology and microstructure of the 15-layer ZnO thin film were investigated by field-emission scanning electron microscopy (FESEM), and the corresponding micrographs are reported in Figure 6 at different magnifications. At low magnification (Figure 6a), the film uniformly covers the substrate over a wide area. The surface appears dense and continuous, with no cracks, pinholes, or large-scale defects. This uniformity

demonstrates that the layer-by-layer deposition yielded a well-coalesced film, free from imperfections that could act as shunt pathways or recombination centers and degrade device performance.

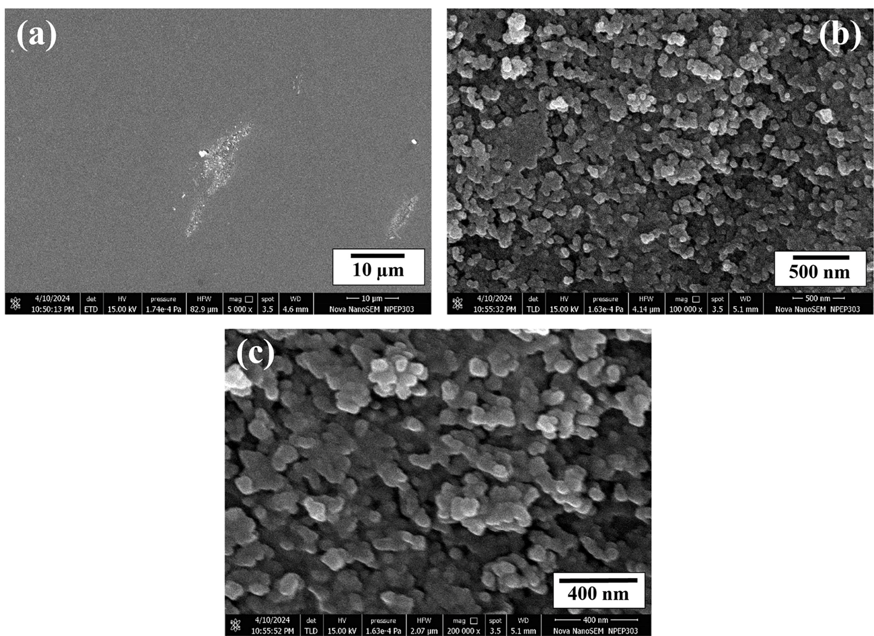

Figure 6. FESEM micrographs of the 15-layer ZnO thin film at different magnifications: (**a**) 5000×, (**b**) 100,000×, and (**c**) 200,000×.

At higher magnifications (Figure 6b,c), the granular structure of the film becomes evident, highlighting the nanoscale features of the crystallites. The surface is polycrystalline, consisting of compact, tightly packed grains with quasi-spherical or slightly faceted geometry, typical of ZnO films grown under these conditions. Grain boundaries are well-defined, and the grain size is relatively uniform, forming a dense and continuous network. This compact arrangement reduces voids between grains, enhances structural integrity, and facilitates charge carrier transport across grain boundaries. The individual grains are composed of agglomerated nanocrystallites that coalesced during the multi-layer deposition and subsequent annealing processes. At the nanoscale, the surface appears smooth, with a regular granular pattern. Such morphology indicates a growth mechanism favoring uniform nucleation followed by vertical and lateral grain growth, ultimately yielding the dense and ordered structure observed. The compact and well-defined grain morphology represents a strong indication of good crystalline quality, which is essential for achieving desirable optical and electrical performance in ZnO-based thin-film devices. Cross-sectional FESEM or transmission electron microscopy (TEM) imaging was not available in the present study, so the internal layering could not be visualized directly. However, the smooth surface morphology and the monotonic evolution of thickness and roughness with layer number suggest that the individual spin coated layers coalesce into a continuous, well-densified film during the final annealing step.

3.4. Photoluminescence Analysis

The photoluminescence properties of ZnO thin films with 5, 10, and 15 layers are reported in Figure 7. These results are analyzed in relation to the thickness and surface roughness data summarized in Table 1 and correlated with the previously discussed optical and structural parameters to provide a comprehensive evaluation of the material quality and defect structure.

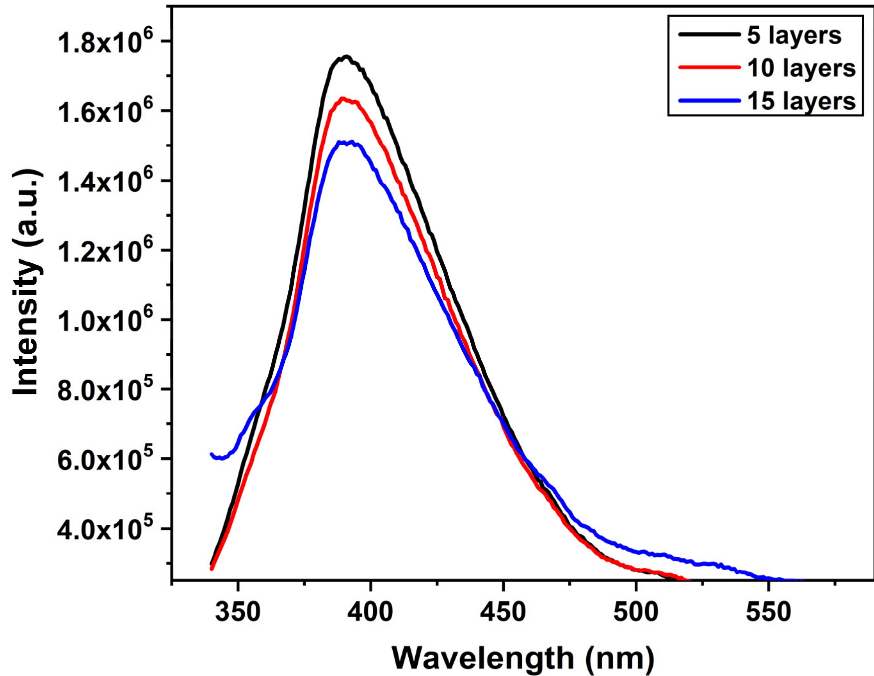

Figure 7. Room-temperature PL spectra of ZnO thin films with 5, 10, and 15 layers under 325 nm excitation.

Table 1. Thickness and RMS surface roughness of ZnO thin films with different numbers of layers.

Number of Layers	Thickness (nm)	Roughness (nm)
5	43.81	5.54
10	51.20	3.10
15	80.68	2.00

As expected, the film thickness increases with the number of deposited layers, from 43.81 nm (5 layers) to 51.20 nm (10 layers) and 80.68 nm (15 layers). More importantly, the RMS surface roughness decreases with increasing thickness: 5.54 nm for the 5-layer film, 3.10 nm for the 10-layer film, and 2.00 nm for the 15-layer film. This reduction indicates improved film uniformity and enhanced grain coalescence, resulting in smoother surface morphology as the film grows [43]. A smoother surface is generally favorable for device applications, as it promotes sharper interfaces and reduces light scattering.

Figure 7 shows the room-temperature PL spectra of the ZnO thin films. All samples exhibit a dominant UV emission peak, characteristic of near-band-edge (NBE) excitonic recombination in ZnO. The NBE peak is centered at approximately 393–395 nm (3.15–3.13 eV) for all thicknesses, consistent with the optical band gap values obtained from absorption spectra (Figure 3c), when considering the exciton binding energy of ZnO (~60 meV) and possible Stokes shifts. A slight redshift of the NBE peak with increasing thickness is noticeable, in agreement with the observed decrease in optical band gap (from 3.26 eV for 5 layers to 3.23 eV for 15 layers), a behavior often associated with improved crystallinity and strain relaxation in thicker films [44].

The intensity of the NBE emission strongly depends on film thickness. The 5-layer film shows the highest NBE intensity, followed by the 10-layer film, whereas the 15-layer film exhibits the lowest intensity. This trend, although counterintuitive given the larger excitation volume of thicker films, suggests the presence of additional non-radiative recombination pathways or enhanced self-absorption effects in thicker layers [4]. This apparent thickness dependence must be interpreted with caution, as PL intensity is also influenced

by optical path length, self-absorption, and the balance between radiative and non-radiative defect-related recombination channels.

Besides the UV emission, all spectra present a broad, low-intensity band in the visible region (approximately 450–550 nm), more similar to a tail than a distinct peak. This visible luminescence is commonly ascribed to deep-level defects within the ZnO band gap, such as oxygen vacancies, zinc interstitials, or zinc vacancies [2,5]. The relative intensity of this defect-related emission with respect to the NBE peak serves as an indicator of crystalline quality and defect density in the films.

3.5. Correlation of Photoluminescence Characteristics with Structural Disorder and Optical Properties

The PL results, particularly the trend in NBE intensity, can be correlated with the Urbach energy (E_u) values determined previously (Figure 5). The 15-layer film, which shows the highest Urbach energy (0.517 eV) and thus the greatest structural disorder, exhibits the lowest NBE PL intensity. This correlation indicates that increased disorder in the 15-layer film enhances the density of non-radiative recombination centers, leading to quenching of the excitonic emission [6].

The 10-layer film presents the lowest Urbach energy (0.431 eV), suggesting a relatively more ordered structure compared to both the 5-layer (0.443 eV) and 15-layer films. However, the 5-layer film displays a higher NBE PL intensity than the 10-layer film. This suggests that although the 5-layer film is slightly more disordered in terms of E_u, the dominant defects responsible for non-radiative recombination may be less effective or less numerous. Additional factors, such as enhanced light extraction due to higher surface roughness (5.54 nm vs. 3.10 nm) or reduced self-absorption in the thinner film, could also contribute to the stronger PL response [7]. The relatively high Urbach energies for all samples (0.431–0.517 eV) indicate a significant density of tail states, consistent with the observed defect-related visible emission.

The progressive reduction in surface roughness with increasing thickness (Table 1) confirms a morphological evolution toward smoother films. While smoother surfaces generally improve interface quality and reduce scattering losses, the dominant factor affecting the NBE PL intensity appears to be the internal quantum efficiency, governed by the density of non-radiative defects. The pronounced reduction in PL intensity in the 15-layer film, despite its lowest surface roughness (2.00 nm), highlights the detrimental role of bulk disorder (as indicated by its high E_u) in limiting radiative efficiency.

In summary, all films exhibit the characteristic NBE emission of ZnO, but its intensity is strongly influenced by the interplay between thickness and structural disorder. The 5-layer film shows the most intense emission, reflecting a favorable balance between excitation volume and non-radiative recombination, despite higher roughness. Conversely, the 15-layer film undergoes significant PL quenching, directly correlated with its increased structural disorder. These findings emphasize the importance of defect control in optimizing the luminescent performance of ZnO thin films for optoelectronic applications. When considered together with the Urbach energy analysis, the PL data indicate that the 10-layer film provides an approximate compromise between surface smoothness, structural order, and defect density. The 15-layer film, although exhibiting lower roughness, accumulates additional deep-level defects that enhance visible emission and non-radiative recombination.

4. Conclusions

In this study, the influence of layer number (5, 10, and 15) on the structural, morphological, and optoelectronic properties of ZnO thin films was systematically investigated. An increase in the number of layers resulted in a predictable rise in film thickness, from

43.81 nm (5 layers) to 80.68 nm (15 layers), accompanied by a significant reduction in surface roughness, from 5.54 nm to 2.00 nm. This trend indicates improved surface homogeneity at the substrate interface, although the bulk defect density does not decrease monotonically with increasing thickness. XRD analysis of the 15-layer film confirmed the polycrystalline hexagonal wurtzite structure.

Optical characterization revealed enhanced UV absorbance and reduced visible transmittance with increasing thickness, along with a slight decrease in the optical band gap from 3.26 eV (5 layers) to 3.23 eV (15 layers). Photoluminescence analysis showed that the 5-layer film exhibited the most intense NBE emission, suggesting an optimal thickness for maximizing radiative recombination efficiency. FESEM observation indicated irregularly shaped particles with a granular or island-like morphology, while the stoichiometric ratio was successfully maintained. However, this apparent optimum must be interpreted with care, since PL intensity is also affected by optical path length, self-absorption and defect-related non-radiative recombination, and the Urbach-energy analysis points to the 10-layer film as having the lowest overall structural disorder.

These results demonstrate that film thickness exerts a strong influence on the structural and optical behavior of nanocrystalline ZnO thin films, including transmittance, band gap, PL emission, and surface morphology. Moreover, key optical parameters such as refractive index, extinction coefficient, optical conductivity, and dielectric constants showed systematic increases with layer number in the visible range, whereas in the UV range their evolution was more complex, reflecting thickness-dependent microstructural effects.

Overall, these findings establish the number of layers as a critical fabrication parameter for tuning the multifaceted properties of ZnO thin films, highlighting their strong potential for application in photodetection and other optoelectronic devices. Although the band gap variation is modest ($\approx$0.03 eV), the associated shifts in the absorption edge and PL peak can still influence the spectral response of UV photodetectors and transparent optoelectronic devices, thereby motivating the fine thickness control discussed in this work.

Author Contributions: Conceptualization, N.N.M., J.V.S. and R.S.K.; methodology, N.N.M. and J.V.S.; validation, J.V.S. and R.S.K.; formal analysis, N.N.M., S.R.P., J.V.S. and R.A.A.; investigation, N.N.M., J.V.S. and R.S.K.; data curation, N.N.M., S.R.P. and R.A.A.; writing—original draft preparation, S.R.P., D.P. and R.A.A.; writing—review and editing, N.N.M., S.R.P., D.P. and R.A.A.; visualization, J.V.S., D.P. and R.A.A.; supervision, S.R.P., J.V.S., R.A.A. and R.S.K. All authors have read and agreed to the published version of the manuscript.

Funding: This research received no external funding.

Data Availability Statement: Data are available on request due to privacy restrictions.

Acknowledgments: N.N.M., J.V.S. and R.S.K. gratefully acknowledge the support provided by Department of Physics, School of Physical Sciences, Kavayitri Bahinabai Chaudhari North Maharashtra University, Jalgaon (MH). D.P. acknowledges the support from the European Union—NextGenerationEU under the National Recovery and Resilience Plan (NRRP), Mission 04, Component 2, Investment 3.1, Project Code: IR0000027—CUP: B33C22000710006—iENTRANCE@ENL: Infrastructure for Energy TRAnsition aNd Circular Economy @EuroNanoLab.

Conflicts of Interest: The authors declare no conflicts of interest.

Abbreviations

The following abbreviations are used in this manuscript:

ALD	Atomic layer deposition
CVD	Chemical vapor deposition
FESEM	Field-emission scanning electron microscope

FWHM	Full width at half maximum
JCPDS	Joint Committee on Powder Diffraction Standards
NBE	Near-band-edge
PL	Photoluminescence
PLD	Pulsed laser deposition
RMS	Root-mean-square
TEM	Transmission electron microscopy
UV	Ultraviolet
XRD	X-ray diffraction

References

1. Wang, Z.L. Zinc oxide nanostructures: Growth, properties and applications. *J. Phys. Condens. Matter* **2004**, *16*, R829–R858. [CrossRef]
2. Özgür, Ü.; Alivov, Y.I.; Liu, C.; Teke, A.; Reshchikov, M.A.; Doğan, S.; Avrutin, V.; Cho, S.-J.; Morkoç, H. A comprehensive review of ZnO materials and devices. *J. Appl. Phys.* **2005**, *98*, 041301. [CrossRef]
3. Klingshirn, C. ZnO: From basics to applications. *Phys. Status Solidi B* **2007**, *244*, 3027–3073. [CrossRef]
4. Muchuweni, E.; Sathiaraj, T.S.; Nyakotyo, H. Synthesis and characterization of zinc oxide thin films for optoelectronic applications. *Heliyon* **2017**, *3*, e00285. [CrossRef]
5. Fortunato, E.; Barquinha, P.; Martins, R. Oxide semiconductor thin-film transistors: A review of recent advances. *Adv. Mater.* **2012**, *24*, 2945–2986. [PubMed]
6. Muslih, E.Y.; Kim, K.H. Preparation of zinc oxide (ZnO) thin film as transparent conductive oxide (TCO) from zinc complex compound on thin film solar cells: A study of O_2 effect on annealing process. *IOP Conf. Ser. Mater. Sci. Eng.* **2017**, *214*, 012001. [CrossRef]
7. Ribut, S.H.; Abdullah, C.A.C.; Mohd Yusoff, M.Z. Investigations of structural and optical properties of zinc oxide thin films growth on various substrates. *Results Phys.* **2019**, *13*, 102146. [CrossRef]
8. Gartner, M.; Stroescu, H.; Mitrea, D.; Nicolescu, M. Various applications of ZnO thin films obtained by chemical routes in the last decade. *Molecules* **2023**, *28*, 4674. [CrossRef]
9. Madhavanunni Rekha, S.; Vadakke Neelamana, H.; Bhat, S.V. Recent advances in solution-processed zinc oxide thin films for ultraviolet photodetectors. *ACS Appl. Electron. Mater.* **2023**, *5*, 4051–4066. [CrossRef]
10. Krysova, H.; Mansfeldova, V.; Tarabkova, H.; Pisarikova, A.; Hubicka, Z.; Kavan, L. High-quality dense ZnO thin films: Work function and photo/electrochemical properties. *J. Solid State Electrochem.* **2024**, *28*, 2531–2546. [CrossRef]
11. Zubkins, M.; Gabrusenoks, J.; Chikvaidze, G.; Aulika, I.; Butikova, J.; Kalendarev, R.; Bikse, L. Amorphous ultra-wide bandgap ZnO_x thin films deposited at cryogenic temperatures. *J. Appl. Phys.* **2020**, *128*, 215303. [CrossRef]
12. Yergaliuly, G.; Soltabayev, B.; Kalybekkyzy, S.; Bakenov, Z.; Mentbayeva, A. Effect of thickness and reaction media on properties of ZnO thin films by SILAR. *Sci. Rep.* **2022**, *12*, 851. [CrossRef]
13. Laurenti, M.; Cauda, V. Porous zinc oxide thin films: Synthesis approaches and applications. *Coatings* **2018**, *8*, 67. [CrossRef]
14. Anilkumar, T.S.; Girija, M.L.; Venkatesh, J. Synthesis and characterization of ZnO thin films. *AIP Conf. Proc.* **2016**, *1728*, 020509. [CrossRef]
15. Sahoo, A.K.; Wu, G.M. Preparation and Characterization of High Quality Zinc Oxide Thin Films for Optoelectronic Applications. In Proceedings of the 2024 International Conference on Artificial Intelligence, Computer, Data Sciences and Applications (ACDSA), Victoria, Seychelles, 1–2 February 2024.
16. Stojanoska, I.; Okorn, M.; Kmet, B.; Uršič, H.; Gradišnik, V.; Čakara, D.; Kovač, J.; Kuscer, D. Indium-zinc-oxide thin films produced by low-cost chemical solution deposition: Tuning the microstructure, optical and electrical properties with the processing conditions. *Heliyon* **2023**, *9*, e19744. [CrossRef]
17. Islam, M.R.; Rahman, M.; Farhad, S.F.U.; Podder, J. Structural, optical and photocatalysis properties of sol–gel deposited Al-doped ZnO thin films. *Surf. Interfaces* **2019**, *16*, 120–126. [CrossRef]
18. Amakali, T.; Daniel, L.S.; Uahengo, V.; Dzade, N.Y.; de Leeuw, N.H. Structural and optical properties of ZnO thin films prepared by molecular precursor and sol–gel methods. *Crystals* **2020**, *10*, 132. [CrossRef]
19. Hussin, R.; Hanafi, F.; Rashid, R.A.; Harun, Z.; Kamdi, Z.; Ibrahim, S.A.; Ainuddin, A.R.; Rahman, W.; Leman, A.M. Structured analysis of nanostructured zinc oxide (ZnO) thin films deposited by sol-gel. *Arch. Metall. Mater.* **2022**, *67*, 1055–1060. [CrossRef]
20. Tseng, M.-C.; Wuu, D.-S.; Chen, C.-L.; Lee, H.-Y.; Chien, C.-Y.; Liu, P.-L.; Horng, R.-H. Characteristics of atomic layer deposition–grown zinc oxide thin film with and without aluminum. *Appl. Surf. Sci.* **2019**, *491*, 535–543. [CrossRef]
21. Zahedi, F.; Dariani, R.S.; Rozati, S.M. Structural, optical and electrical properties of ZnO thin films prepared by spray pyrolysis: Effect of precursor concentration. *Bull. Mater. Sci.* **2014**, *37*, 433–439. [CrossRef]

22. Chongsri, K.; Bangbai, C.; Techitdheera, W.; Pecharapa, W. Characterization and photoresponse properties of Sn-doped ZnO thin films. *Energy Procedia* **2013**, *34*, 721–727. [CrossRef]
23. Prasada Rao, T.; Santhoshkumar, M.C. Effect of thickness on structural, optical and electrical properties of nanostructured ZnO thin films by spray pyrolysis. *Appl. Surf. Sci.* **2009**, *255*, 4579–4584. [CrossRef]
24. Mullings, M.N.; Hägglund, C.; Tanskanen, J.T.; Yee, Y.; Geyer, S.; Bent, S.F. Thin film characterization of zinc tin oxide deposited by thermal atomic layer deposition. *Thin Solid Film.* **2014**, *556*, 186–194. [CrossRef]
25. Jayaraj, M.K.; Saji, K.J.; Nomura, K.; Kamiya, T.; Hosono, H. Optical and electrical properties of amorphous zinc tin oxide thin films examined for thin film transistor application. *J. Vac. Sci. Technol. B* **2008**, *26*, 495–501. [CrossRef]
26. Abdel-Galil, A.; Hussien, M.S.A.; Yahia, I.S. Synthesis and optical analysis of nanostructured F-doped ZnO thin films by spray pyrolysis: Transparent electrode for photocatalytic applications. *Opt. Mater.* **2021**, *114*, 110894. [CrossRef]
27. Taunk, P.B.; Das, R.; Bisen, D.P.; Tamrakar, R.K.; Rathor, N. Synthesis and optical properties of chemical bath deposited ZnO thin film. *Karbala Int. J. Mod. Sci.* **2015**, *1*, 159–165. [CrossRef]
28. Chaitra, U.; Kekuda, D.; Rao, K.M. Effect of annealing temperature on the evolution of structural, microstructural, and optical properties of spin coated ZnO thin films. *Ceram. Int.* **2017**, *43*, 7115–7122. [CrossRef]
29. Rochdi, N.; El Boujlaidi, A.; Afkir, A.; Vega, E.; Yagoubi, S.; El Gabbas, Y. Deposition and properties of $ZnSiO_3$-containing zinc oxide thin films reactively sputtered at room temperature. *Thin Solid Film.* **2020**, *709*, 138218. [CrossRef]
30. Khan, M.T.; Prasad, K.H.; Khan, A.; Shkir, M. Enhancement of photodetector performance of aluminum-doped zinc oxide thin films fabricated via SILAR method: Structural, optical, and electrical analysis. *Inorg. Chem. Commun.* **2024**, *169*, 112973. [CrossRef]
31. Siva, N.; Sakthi, D.; Ragupathy, S.; Arun, V.; Kannadasan, N. Synthesis, structural, optical and photocatalytic behavior of Sn doped ZnO nanoparticles. *Mater. Sci. Eng. B* **2020**, *253*, 114497. [CrossRef]
32. Ahmed, G.; Mohamed, W.S.; Hasaneen, M.F.; Ali, H.M.; Ibrahim, E.M.M. Optical, structural, electrical and photocatalytic properties of aluminum doped zinc oxide nanostructures. *Opt. Mater.* **2023**, *140*, 113880. [CrossRef]
33. Sandeep, K.M.; Bhat, S.; Dharmaprakash, S.M. Structural, optical, and LED characteristics of ZnO and Al doped ZnO thin films. *J. Phys. Chem. Solids* **2017**, *104*, 36–44. [CrossRef]
34. Ayana, A.; Gummagol, N.B.; Patil, P.S.; Sharma, P.; Rajendra, B.V. Nonlinear optical properties of zinc oxide thin films. *Opt. Laser Technol.* **2024**, *175*, 110820. [CrossRef]
35. Khan, M.I.; Bhatti, K.A.; Qindeel, R.; Alonizan, N.; Althobaiti, H.S. Characterizations of multilayer ZnO thin films deposited by sol-gel spin coating technique. *Results Phys.* **2017**, *7*, 651–655. [CrossRef]
36. Ahmed, Z.; Padha, N.; Padha, B.; Hussain, Z.; Singh, D. Dynamics of ALD-grown ZnO thin films with varying thicknesses and substrate temperatures for optoelectronic applications. *Opt. Quantum Electron.* **2025**, *57*, 336. [CrossRef]
37. Rajkumar, C.; Arulraj, A. Enhanced photoconductive response of ZnO thin films with the impact of annealing temperatures on structural and optical properties. *Sci. Rep.* **2025**, *15*, 28851. [CrossRef] [PubMed]
38. Zahedi, F.; Dariani, R.S.; Rozati, S.M. Effect of substrate temperature on the properties of ZnO thin films prepared by spray pyrolysis. *Mater. Sci. Semicond. Process.* **2013**, *16*, 245–249. [CrossRef]
39. Jlassi, M.; Sta, I.; Hajji, M.; Ezzaouia, H. Effect of nickel doping on physical properties of zinc oxide thin films prepared by the spray pyrolysis method. *Appl. Surf. Sci.* **2014**, *301*, 216–224. [CrossRef]
40. Sung, N.-E.; Lee, K.-S.; Lee, I.-J. Structural characterization of Zr-doped ZnO films deposited on quartz substrates by reactive radio frequency magnetron co-sputtering. *Thin Solid Film.* **2018**, *651*, 42–47. [CrossRef]
41. Gonçalves, R.S.; Barrozo, P.; Cunha, F. Optical and structural properties of ZnO thin films grown by magnetron sputtering: Effect of the radio frequency power. *Thin Solid Film.* **2016**, *616*, 265–269. [CrossRef]
42. Aparna, C.; Mahesha, M.G.; Karunakara, N.; Yashodhara, I.; Shetty, P.K. Structural, optical, and electrical characteristics of gamma-irradiated Zn-doped indium oxide thin films for sensor applications. *Opt. Mater.* **2025**, *167*, 117348. [CrossRef]
43. Yasmin, F.; Sheikh, M.S.; Bhuiyan, A.H.; Rahman, M.J. A comprehensive study on structural and optical properties of zinc selenide/poly ortho-methoxyaniline hybrid thin films deposited by chemical bath deposition and plasma polymerization techniques. *Arab. J. Chem.* **2024**, *17*, 105842. [CrossRef]
44. Tian, J.-L.; Zhang, H.-Y.; Wang, G.-G.; Wang, X.-Z.; Sun, R.; Jin, L.; Han, J.-C. Influence of film thickness and annealing temperature on the structural and optical properties of ZnO thin films on Si (100) substrates grown by atomic layer deposition. *Superlattices Microstruct.* **2015**, *83*, 719–729. [CrossRef]

Disclaimer/Publisher's Note: The statements, opinions and data contained in all publications are solely those of the individual author(s) and contributor(s) and not of MDPI and/or the editor(s). MDPI and/or the editor(s) disclaim responsibility for any injury to people or property resulting from any ideas, methods, instructions or products referred to in the content.